Freeze-protection economics can reverse the heat-transfer-fluid preference for cold high-altitude parabolic-trough concentrating solar power: a four-dimensional (4E) and thermal-storage market-value assessment

Zhaohui Han[a,*], Zengli Dai[a], Yuan Wei[a], Yu Xie[a], Dongxiang Wang[a]

[a] *SEPCOIII Electric Power Construction Co., Ltd., Qingdao, 266100, Shandong, China*

Abstract

Heat-transfer-fluid (HTF) selection for parabolic-trough concentrating solar power is usually settled at sea level, yet a growing share of new capacity sits on high plateaus where reduced air density and low temperatures reshape both heat loss and freeze protection. We assess molten salt (Solar Salt) against thermal oil (Therminol VP-1) for a parabolic-trough plant at Golmud (2801 m, Qinghai) using a four-dimensional (energy, exergy, economic, environmental) framework coupled to a thermal-storage market-value model with time-of-use pricing. Altitude-dependent air properties are propagated through the receiver heat-loss model, molten-salt freeze parasitics, and component-level exergy. The direct altitude effect on collector heat loss is small (~0.2%), because reduced convective loss is largely offset by increased radiative loss; freeze protection, by contrast, is the dominant controllable penalty for molten salt, requiring roughly 20 times the maintenance power of thermal oil. Under a CNY cost basis anchored to recent Chinese large-scale CSP data, an idealized clear-sky comparison reproduces the conventional preference for molten salt (levelized cost 480 versus 523 CNY/MWh at each fluid's optimal storage). But when the freeze penalty is charged on realistic typical-meteorological-year weather, the ranking reverses: the salt's levelized cost rises to about 1040 CNY/MWh against 870 for the oil, because cold-weather freeze protection and lower net output erase the storage-cost advantage. The decisive driver is therefore not elevation-induced air-density change by itself but freeze-protection economics under cold plateau weather; mitigating that penalty – for example with lower-melting salts – is the key route to restoring molten salt's storage advantage.

Keywords: parabolic trough collector, molten salt, high-altitude CSP, freeze protection, levelized cost of energy, thermal energy storage, heat transfer fluid

1. Introduction

Parabolic-trough plants are the most commercially mature concentrating solar power technology, and the choice of heat-transfer fluid (HTF) – traditionally a synthetic oil, increasingly

*Corresponding author. Email address: hanzhaohui@sepco3.com.

Email addresses: hanzhaohui@sepco3.com (Zhaohui Han), dzl@sepco3.com (Zengli Dai), yuan.wei@sepco3.com (Yuan Wei)

a molten nitrate salt – sets the plant's operating temperature, storage architecture, and much of its cost [1, 2, 3, 4]. Molten salt permits a higher turbine-inlet temperature and cheap direct two-tank storage but must be kept far above ambient to avoid freezing; thermal oil has a much lower freezing threshold but caps the temperature and needs an oil-to-salt heat exchanger to store heat [5, 6]. Which fluid is preferable is usually decided from sea-level performance and a levelized-cost comparison.

Two developments unsettle that decision. The first is geographic: a large and growing share of new trough capacity is being built on the high plateaus of western China, with plants at Golmud, Delingha, and across Qinghai and Tibet sitting between roughly 2800 and 4000 m [7, 8]. At those elevations the air is a quarter to a third less dense than at sea level and ambient temperatures are low, so both the receiver heat loss and the freeze-protection burden depart from their sea-level values. The second is economic: as CSP is valued increasingly for dispatchable, peak-coincident generation rather than bulk energy, the market *value* of thermal storage – not only its levelized cost – has become central to plant design [9, 10].

Neither development is reflected in standard trough models. Altitude is almost absent from the trough-modelling literature: conventional models hardcode sea-level air properties, the most recent comprehensive review of trough heat loss lists neither elevation nor air pressure among its influencing factors [11], and the one systematic altitude study we are aware of treats flat-plate collectors and the receiver rather than a trough's optics or its fluid choice [12]. Four-dimensional (energy–exergy–economic–environmental, 4E) analyses of trough collectors are by now common [13, 14], but they typically optimise a working fluid or a power cycle rather than weigh heat-transfer-fluid choice against storage market value, and none does so at altitude.

This paper assesses molten salt against thermal oil for a high-altitude trough plant within a single framework that closes these gaps. Altitude-dependent air properties are propagated through a Forristall receiver heat-loss model, molten-salt freeze parasitics, and a component-level exergy analysis; these feed a four-dimensional (4E) scorecard and a thermal-storage market-value model with time-of-use pricing. Using Golmud (2801 m) as the demonstration site, we find that the direct air-density effect of elevation on heat loss is small, but that cold plateau weather changes the annual balance once freeze protection is charged: the conventional cost preference for molten salt holds under idealized clear-sky conditions and *reverses* – thermal oil becoming the cheaper option – under typical-meteorological-year operation at Golmud. The decision is therefore governed by freeze-protection economics under cold-site operation, with a lower-freezing-point salt the clear priority for improvement. The aperture-scale optical design of the collector is treated in a companion paper [15]; here the aperture is held at the 5.77 m reference.

2. Site, system, and methodology

We model a parabolic-trough plant with two-tank thermal storage and a steam-Rankine power block, configured identically for the two candidate heat-transfer fluids (HTFs) except where the fluid itself dictates otherwise. The collector geometry is fixed to the EuroTrough/LS-3 reference (5.77 m aperture); aperture-scale optical design – larger apertures, the intercept factor, and its coupling to altitude through wind load – is the subject of the companion paper [15] and is held constant here, so that altitude enters the present study only through the air-property, heat-loss, and freeze-protection channels. The full chain is implemented as a configuration-driven, openly available Python code (see Data availability), and every quantitative claim below is reproducible from it.

2.1. Site and weather

The study site is Golmud, Qinghai (36.42°N, 94.9°E, 2801 m), representative of the high plateaus across western China where most new trough capacity is being built [7, 8]. Two irradiance scenarios are used and each is evaluated both at the site elevation and, for comparison, at sea level: a clear-sky reference generated with the REST2 model [16], and a typical-meteorological-year (TMY) series [17]. The design point uses a direct normal irradiance of $900\,\mathrm{W\,m^{-2}}$. Solar Salt is operated between 290 and 540 °C and Therminol VP-1 between 290 and 390 °C, the upper limits set by salt stability and oil cracking respectively. We deliberately separate elevation from weather in the scenario design: air-density effects enter the receiver model through Section 2.2, whereas the cost-ranking reversal is attributed only after comparing clear-sky, TMY-without-freeze, and TMY-with-freeze cases in Section 5.1.

2.2. Altitude-dependent air properties

Conventional trough models hardcode sea-level air properties. We instead make the air density, and the convective heat-transfer correlations that depend on it, explicit functions of elevation. Treating air as an ideal gas, the density follows the U.S. Standard Atmosphere (1976) pressure–altitude relation [18],

$$\rho(z) = \frac{p(z)}{R_a T}, \qquad p(z) = p_0 \left(1 - 2.25577 \times 10^{-5}\, z\right)^{5.25588}, \tag{1}$$

while the dynamic viscosity, thermal conductivity, and Prandtl number are functions of temperature alone (Sutherland's law [19] and a conductivity power law), independent of pressure. At Golmud the pressure is 0.71 of its sea-level value, so the density is about 29% lower and the kinematic viscosity $\nu = \mu/\rho$ about 41% higher than the sea-level value a conventional model would assume. The clear-sky radiative sink uses the Swinbank sky temperature [20, 21].

2.3. Collector, receiver, power block, and storage models

The receiver heat loss is computed from a one-dimensional steady energy balance on the heat-collection element following Forristall [22] and consistent with heat-loss measurements of the PTR70 receiver class [23], resolving conduction, convection, and radiation from the absorber across the evacuated glass envelope to the surroundings by standard correlations [24]; external convection from the envelope uses the Churchill–Bernstein correlation [25], into which the altitude-corrected air properties of Section 2.2 enter. The collector loop sets the mass flow required to reach the fluid outlet temperature and returns the field thermal efficiency. Thermal storage is two-tank: Solar Salt serves as both HTF and storage medium (direct storage), whereas Therminol VP-1 requires a separate salt inventory and an oil-to-salt heat exchanger (indirect storage), which imposes both an approach-temperature exergy penalty and an additional capital cost [6, 5]. The steam-Rankine power-block efficiency is a function of turbine-inlet temperature, which favours the higher-temperature salt (540 versus 390 °C). Fluid properties for Solar Salt (a 60–40 $NaNO_3$–KNO_3 mixture) and Therminol VP-1 are taken from standard compilations [4, 26, 27]. In the annual freeze calculation Solar Salt is conservatively assigned a 238 °C model freeze threshold, matching the lower validity bound of the property correlations, plus a 12 °C guard margin; Therminol VP-1 uses 12 °C plus the same guard. This guard-temperature contrast is the origin of the freeze-protection asymmetry quantified in Section 3.3.

The plant is sized as a single collector loop – aperture area $3462\,\mathrm{m^2}$ ($5.77\,\mathrm{m} \times 600\,\mathrm{m}$) delivering $2.16\,\mathrm{MW_{th}}$ at the design point – operated at a solar multiple of 2.5: the field is oversized

2.5× relative to the power block (rated thermal input 0.865 MW_{th}, nameplate ≈0.34 MW_e) so that midday surplus charges storage, and each hour of storage holds 865 kWh_{th}. This is a single-loop demonstration scale; all absolute energies and capital costs scale with it, but the molten-salt-versus-oil comparison does not. Capital cost (Section 4) is then assembled from this geometry and the unit costs, making every LCOE reproducible.

2.4. Independent literature consistency checks

No single experiment exercises the full altitude-coupled 4E chain, so we check the model against five independent published results, each at the level of *direction and magnitude* rather than absolute numerical agreement – a closer parity would require reproducing device-specific geometries that we do not model. (i) The altitude heat-loss mechanism – convective loss falling and radiative loss rising with elevation – reproduces the trend reported by Wang et al. for flat-plate collectors [12]; their radiation-dominated flat-plate balance is not numerically comparable to the convection-dominated evacuated trough receiver here, and that very gap (no altitude-resolved heat-loss decomposition exists for trough receivers) is part of what this paper fills. (ii) The receiver cool-down time inferred from the modelled heat loss (∼4.9 h to the salt freezing point) is of the same order as the ∼4 h measured by Russo et al. [28]. (iii) The second-law ranking of the two fluids (salt above oil) matches Khandelwal et al. [29]. (iv) The idealized clear-sky levelized cost (∼0.48 CNY/kWh) is consistent with the 0.47–0.53 CNY/kWh band reported for current Chinese large-scale plants [8]; we stress that the unit costs were *anchored* to that band, so this is a calibration consistency check, not an independent validation (and the realistic levelized cost is substantially higher, Section 5.1). (v) The pressure–altitude relation of Eq. (1) matches the U.S. Standard Atmosphere to within 1% [18]. These are consistency tests that bound the model's behaviour, not a validation of absolute accuracy; all five are encoded as regression tests in the released code.

3. Component physics under altitude

Before assembling the 4E scorecard we examine how altitude enters each physical channel at the design point. Three effects compete – a small reduction in convective heat loss, a negligible change in design-point efficiency, and a large, altitude-insensitive freeze-protection burden for molten salt – and it is their interplay, not any single one, that drives the fluid comparison.

3.1. Convective heat loss and its altitude correction

At the design wind speed (3 m s^{-1}) the evacuated receiver loses heat predominantly by convection from the glass envelope: convection accounts for 65–69% of the total of about 263 W m^{-1}, the remainder being radiation (Fig. 1). Raising the site from near sea level to 2801 m lowers the air density by 29% and raises the kinematic viscosity by 41% (Section 2.2), which cuts the convective loss from 181 to 172 W m^{-1}. The glass envelope then runs slightly hotter, so the radiative loss rises from 82 to 91 W m^{-1}, and the two changes nearly cancel: the total receiver loss falls by only 0.2% (263.2 to 262.7 W m^{-1}), and the field-level heat loss for Solar Salt by 0.24% (174.2 to 173.8 kW). The altitude effect on the *magnitude* of heat loss is therefore small, but its *partitioning* shifts materially – the convective fraction drops from 69% to 65% between 110 and 2801 m. This is precisely the shift a sea-level-hardcoded model misses, and, as noted in Section 2.4, no altitude-resolved heat-loss decomposition has previously been reported for a trough receiver.

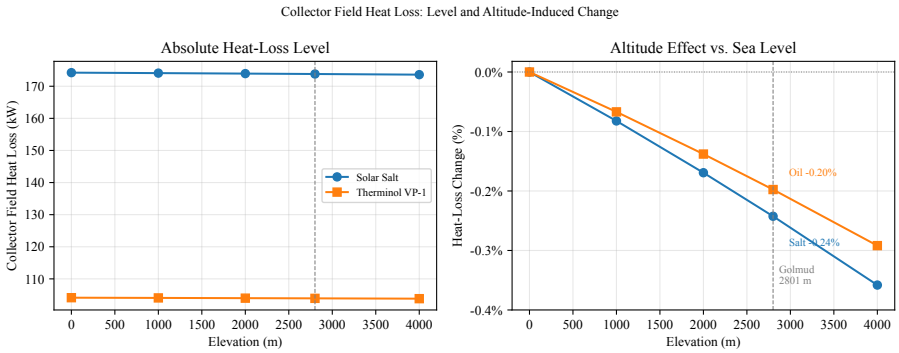

Figure 1: Total collector-field heat-loss level and altitude-induced relative change versus elevation for Solar Salt and Therminol VP-1; altitude enters through the convective channel, but the net change is small because rising radiative loss offsets it.

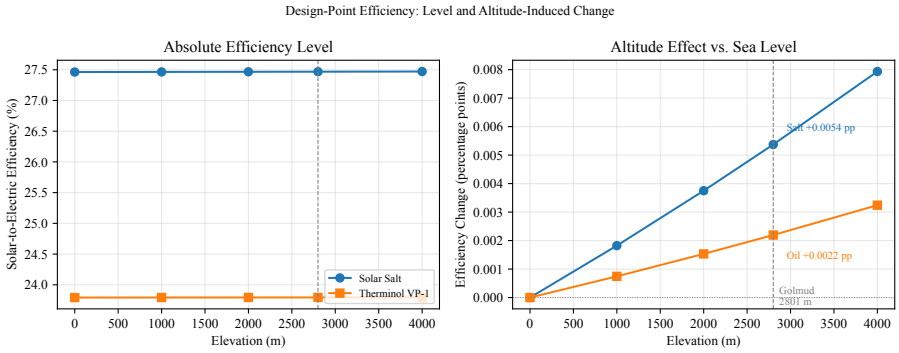

Figure 2: Design-point solar-to-electric efficiency level and altitude-induced change versus elevation for Solar Salt and Therminol VP-1.

3.2. Design-point efficiency versus altitude

Because the heat-loss change is small, the design-point solar-to-electric efficiency is essentially flat with elevation (Fig. 2). It rises imperceptibly as the receiver loss falls – for Solar Salt from 27.463% at sea level to 27.468% at Golmud and 27.471% at 4000 m, a gain of only 0.005–0.008 percentage points – and similarly for Therminol VP-1. The fluids differ far more from each other than either does across altitude: Solar Salt reaches 27.5% against 23.8% for Therminol VP-1, a 3.7-point margin set by the higher turbine-inlet temperature the salt permits (540 versus 390 °C) and hence the higher power-block efficiency (44.0% versus 36.9% gross). The practical message of Fig. 2 is therefore negative but useful: at the design point, altitude neither helps nor hurts conversion efficiency appreciably, so the altitude-sensitive part of the fluid comparison lies elsewhere – in freeze protection and in the annual, weather-dependent energy yield.

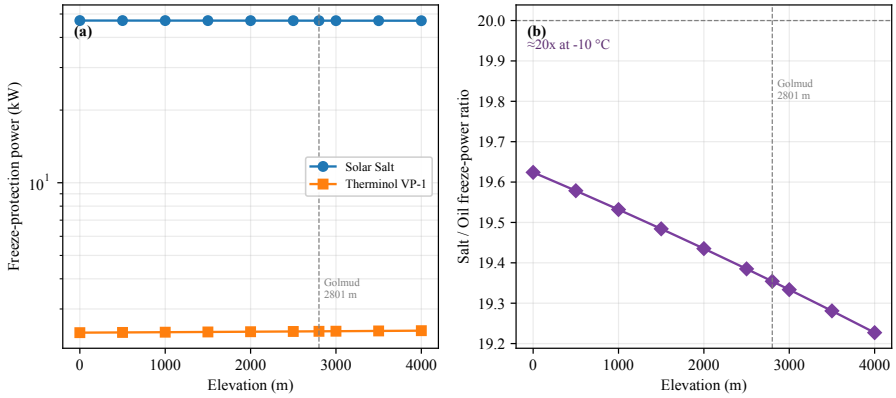

Figure 3: Freeze-protection parasitic power and salt/oil power ratio versus elevation ($T_{\mathrm{amb}} = -10\,^{\circ}\mathrm{C}$). Panel (a) uses a common logarithmic power axis to show the order-of-magnitude gap directly; panel (b) shows that molten salt requires ~20× the maintenance power of thermal oil and that the ratio is nearly altitude-insensitive.

3.3. Molten-salt freeze-protection parasitics

The fluids' modeled guard temperatures differ by more than 200 °C (250 versus 24 °C), and this is molten salt's dominant penalty. To keep the salt above its guard temperature when the field is idle, the receiver must be supplied with about 47 kW of freeze-protection power at the design ambient (−10 °C), against only 2.4 kW for the oil – a ratio of roughly 20 (Fig. 3). Two features of this penalty matter. First, it is almost *insensitive to altitude*: the cold-tube loss is radiation-dominated and radiation is pressure-independent, so the salt's freeze power varies by less than 0.2% from sea level to 4000 m. The high-altitude burden therefore enters not through the air density but through ambient temperature, and the salt/oil ratio itself ranges from about 16 at −20 °C to 25 at 0 °C as the oil's smaller loss falls faster in relative terms. Second, the penalty is paid whenever the field cannot collect, so it accumulates over the cold, cloudy periods typical of plateau sites: the annual freeze-protection energy for Solar Salt at Golmud reaches 200 MWh under clear-sky and 245 MWh under TMY irradiance, against essentially zero (clear-sky) to 9 MWh (TMY) for the oil. This annual burden, not the design-point heat loss, is what makes cold high-altitude operation consequential for the fluid choice.

3.4. Component-level exergy analysis

A first-law efficiency rewards the salt for its higher temperature without charging it for the irreversibility that temperature creates, so we also track the second law. Taking the solar exergy from the Petela relation [30] and the reference temperature as the local ambient, the exergy delivered by each component is $\dot{Q}\,(1 - T_0/T)$ and the destruction in a component is the difference between its inlet and outlet exergy [31]. Figure 4 shows the resulting breakdown at the Golmud design point. The exergy efficiency is 29.5% for Solar Salt against 25.6% for Therminol VP-1: the salt's higher delivery temperature outweighs its slightly larger optical and field losses, confirming the second-law ranking reported elsewhere for these fluids [29]. The largest destruction sits in the optical and collector-field stage and in the power block; the storage stage is negligible at the design point for both fluids (Fig. 4). The oil's indirect arrangement adds an oil-to-salt

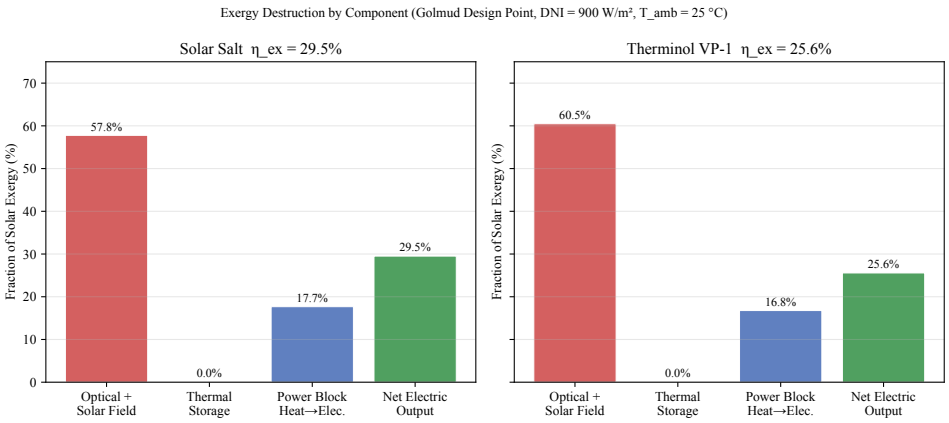

Figure 4: Component-level exergy-destruction breakdown at the Golmud design point (DNI = 900 W m^{-2}, T_0 = 25 °C).

heat-exchanger approach-temperature penalty, but it appears in off-design operation and in capital cost rather than in this design-point snapshot. This design-point advantage for the salt is, in any case, eroded annually by freeze downtime, a tension we quantify in Section 4.

4. Four-dimensional (4E) framework

The four dimensions – energy, exergy, economic, and environmental – are now combined into a single fluid comparison, carrying the design-point physics of Section 3 to annual operation over the two weather scenarios and two elevations.

Energy.. Annual net electricity (Fig. 5, Table 1) reverses part of the design-point story. At sea level under clear skies Solar Salt leads, generating 2611 MWh against 2471 for the oil. At altitude the lead narrows, and under the cloudier TMY irradiance at Golmud it *inverts*: the salt delivers only 897 MWh against the oil's 1073, because its 245 MWh of freeze-protection energy is incurred precisely when irradiance is scarce. The first-law message is therefore conditional – the salt's higher conversion efficiency wins when the sun is reliable, but its freeze burden can dominate under adverse plateau weather.

Exergy.. The same tension appears in the second law: the annual exergy efficiency favours the salt under clear skies (19.8% versus 19.3% at Golmud) but the oil under TMY (17.6% versus 14.7%), again driven by freeze downtime (Table 1). The salt's design-point second-law advantage (Section 3.4) is thus real but weather-contingent.

Economics.. The economic dimension is the levelized cost of energy (LCOE). Capital cost sums the solar field (1200 CNY m^{-2}), thermal storage, and the power block (7.8×10^6 CNY MW^{-1}); storage costs 155 CNY kWh$_{\mathrm{th}}^{-1}$ for the direct-salt system and 295 CNY kWh$_{\mathrm{th}}^{-1}$ for the indirect-oil system, the 140 CNY kWh$_{\mathrm{th}}^{-1}$ difference being the oil-to-salt heat exchanger. These figures follow the cost structure of Turchi and Heath [32], broadly in line with international CSP cost benchmarks [33], converted to CNY and anchored to the 13 500–15 800 CNY kW^{-1} unit investment and 0.47–0.53 CNY kWh^{-1} LCOE reported for current Chinese large-scale plants [8]. With fixed

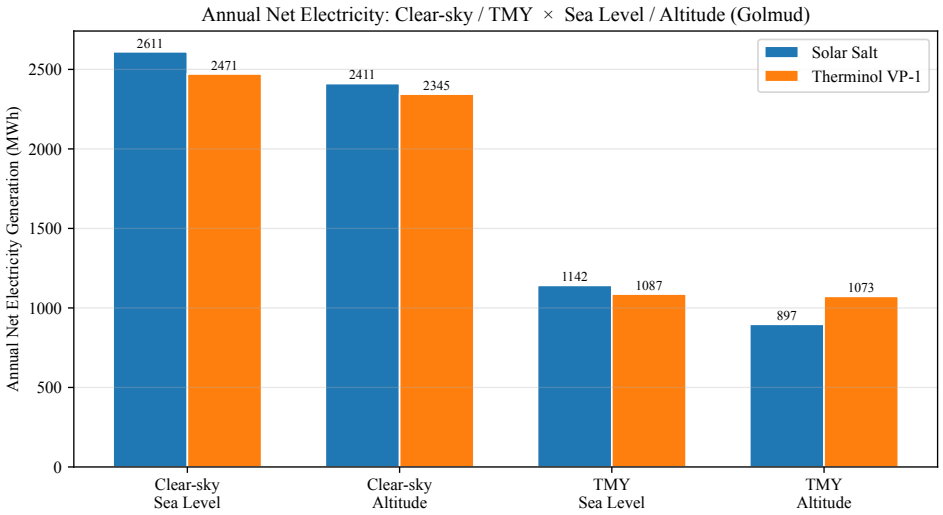

Figure 5: Annual net electricity under clear-sky and TMY irradiance, at sea level and at Golmud, for Solar Salt and Therminol VP-1.

operation and maintenance at 2% of capital, a discount rate of 8%, and a 30-year life, the LCOE is $(\mathrm{CAPEX}\cdot\mathrm{CRF}+\mathrm{O\&M})/E_{\mathrm{net}}$, where the capital recovery factor $\mathrm{CRF}=r(1+r)^n/[(1+r)^n-1]$. Under the idealized clear-sky comparison the salt LCOE is 0.48 CNY kWh^{-1}, within the reported band; under realistic weather it is substantially higher (Section 5.1). Its strong dependence on storage duration *and weather* is the subject of Section 5.

Environment.. Displacing grid electricity at the Chinese grid average of 0.58 kg CO_2 kWh^{-1} [34], the plant avoids about 1000 t CO_2 per year for the salt at 6 h storage on the idealized clear-sky basis (Section 5); under realistic weather the avoided CO_2 scales down with generation. Water use, dominated by mirror washing and any wet cooling, is comparable for the two fluids and is not a discriminator; we therefore carry CO_2 as the environmental metric.

5. Thermal-storage market value

Thermal storage is the principal lever a CSP plant has over both its cost and the market value of its output, and the two move in opposite directions with storage duration. We price generation against a three-tier time-of-use tariff – 1.2, 0.6, and 0.3 CNY kWh^{-1} in peak (10:00–12:00 and 18:00–20:00), flat, and valley hours – and dispatch storage to peak hours first. The market value factor is the revenue-weighted average price divided by the flat price, so a value factor above unity means storage is shifting energy into higher-priced hours.

To isolate the storage-cost mechanism, we first compare the fluids under an *idealized* clear-sky year at a mild constant ambient (+10 °C), in which neither fluid incurs a freeze penalty. Under these conditions, adding storage raises the value factor but also the capital cost, and the LCOE is U-shaped in storage duration (Fig. 6, Table 2). For Solar Salt it falls from 571 CNY MWh^{-1} at no storage to a minimum of 480 CNY MWh^{-1} at 6 h, then rises as further capacity is underused. For Therminol VP-1 the minimum is shallower, comes earlier (3 h, 523 CNY MWh^{-1}), and is higher

Table 1: Annual performance over four scenarios at the baseline plant configuration (Section 2.3); the storage-value sweep of Section 5 sizes storage separately, so its absolute generation differs. Net electricity is after freeze-protection parasitics; η is the *annual average* solar-to-electric efficiency (distinct from the design-point value of Section 3.2) and η_{ex} the annual exergy efficiency (Golmud cases).

Scenario	Fluid	E_{net} (MWh)	η	Freeze (MWh)	η_{ex}
Clear-sky, sea level	Solar Salt	2610.7	0.200	—	—
	Therminol VP-1	2471.2	0.189	—	—
Clear-sky, Golmud	Solar Salt	2410.8	0.185	200.1	0.198
	Therminol VP-1	2344.7	0.180	0.0	0.193
TMY, sea level	Solar Salt	1141.8	0.175	—	—
	Therminol VP-1	1087.2	0.166	—	—
TMY, Golmud	Solar Salt	897.2	0.137	244.6	0.147
	Therminol VP-1	1072.9	0.164	8.7	0.176

Table 2: Annual net electricity, market value factor, LCOE, and avoided CO_2 versus thermal-storage duration (solar multiple 2.5).

Fluid	Storage (h)	E_{net} (MWh)	Value factor	LCOE (CNY/MWh)	CO_2 (t/yr)
Solar Salt	0	1301.3	1.256	570.9	754.7
	3	1602.5	1.270	490.9	929.4
	6	1731.3	1.243	**479.6**	1004.1
	9	1736.1	1.242	503.5	1006.9
	12	1736.4	1.241	528.6	1007.1
Therminol VP-1	0	1237.4	1.256	568.9	717.7
	3	1510.4	1.269	**523.0**	876.0
	6	1625.4	1.243	538.9	942.7
	9	1629.2	1.242	590.4	944.9
	12	1629.3	1.242	643.1	945.0

at every longer duration – 539 against 480 CNY MWh^{-1} at 6 h. The mechanism is the storage architecture: the oil's indirect two-tank arrangement makes each stored kilowatt-hour more expensive, so the oil can neither afford as much storage nor match the salt's cost for the storage it does carry. Taken alone, this idealized comparison reproduces the conventional preference for molten salt – but, as Section 5.1 shows, it does not survive realistic weather.

The market value factor rises to a peak of 1.270 at 3 h, then declines slightly, and is nearly identical for the two fluids at every duration (Table 2); it is set by dispatch against the tariff rather than by the fluid, so it locates a moderate-storage window (3–6 h) but does not discriminate between the candidates. We therefore carry LCOE as the economic metric; Table 2 lists the underlying figures.

5.1. The freeze penalty reverses the cost ranking under realistic weather

The clear-sky comparison above excludes the freeze parasitic that Section 3.3 identified as molten salt's dominant penalty. We therefore repeat the storage sweep under the typical-meteorological-year irradiance and the real ambient temperatures of the Golmud site, so that the

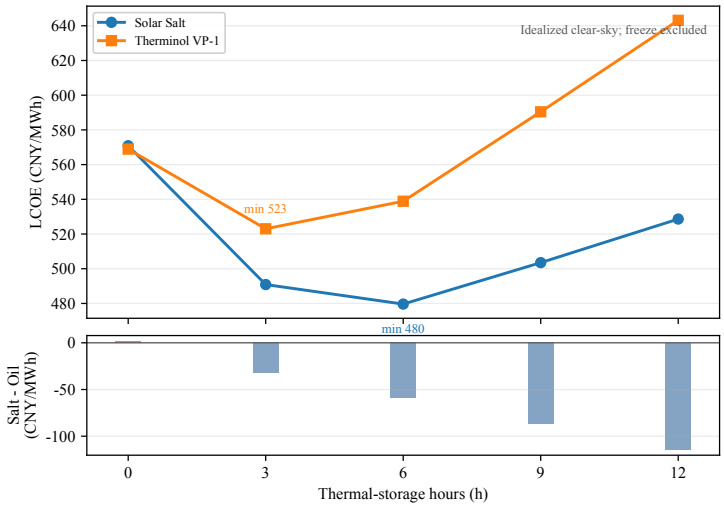

Figure 6: LCOE versus thermal-storage hours under the *idealized* clear-sky comparison (freeze excluded), isolating the storage-cost mechanism. The upper panel shows the U-shaped cost curves; the lower panel shows the salt–oil cost gap on a separate axis. Under this idealized assumption molten salt is cheaper at 6 h (479.6 versus 538.9 CNY/MWh), whereas Table 3 and Section 5.1 give the realistic freeze-included ranking, which reverses.

salt actually pays its freeze cost on cold, sunless hours. This is a three-step attribution test rather than a single altitude comparison: the idealized clear-sky case isolates storage cost, the TMY-without-freeze case adds the weather resource, and the TMY-with-freeze case adds the parasitic. The ranking reverses (Fig. 7, Table 3). Two changes separate the idealized and realistic cases – the irradiance series (clear-sky to TMY) and the freeze charge – and Fig. 7(b) isolates them at 6 h storage. Moving to TMY irradiance roughly doubles both fluids' LCOE but *preserves* the salt's lead (796 versus 883 CNY MWh^{-1} for salt and oil); it is the freeze charge that reverses the ranking, lifting the salt to 1040 while leaving the oil at 891. The mechanism is that the salt's net generation falls far more steeply than the oil's – its 6 h output drops from 1731 to 798 MWh, against 1625 to 983 MWh for the oil – so under realistic weather the salt's LCOE exceeds the oil's at every storage duration (1040 at its 6 h optimum, against the oil's 868 at 3 h). Under realistic plateau weather, thermal oil is the cheaper option, by a margin that is robust in sign across the storage sweep though within the absolute techno-economic uncertainty. The conventional sea-level preference for molten salt is thus an artefact of neglecting freeze: once it is charged on the same weather that produces the generation, the fluid choice at a cold high-altitude site is governed by freeze-protection economics, and it inverts.

Because this conclusion depends on the freeze-protection threshold, we also vary the guard margin from 0 to 18 °C around the modeled freeze point. The sign does not change: at 6 h storage the realistic salt–oil LCOE gap remains positive, ranging from +126 CNY MWh^{-1} at zero guard margin to +163 CNY MWh^{-1} at an 18 °C guard margin; at 3 h storage the gap ranges from +206 to +251 CNY MWh^{-1}. Thus the oil preference under Golmud TMY weather is not created by the particular 12 °C guard margin, although the absolute LCOE gap is sensitive to that operational

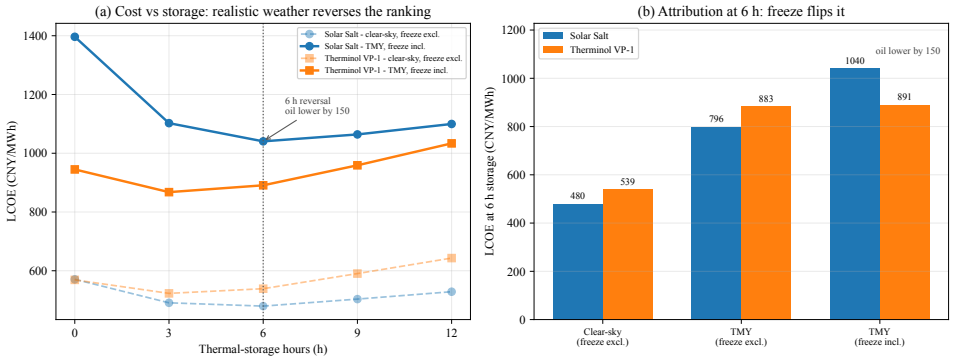

Figure 7: Honest LCOE comparison. (a) LCOE versus storage duration for both fluids under the idealized clear-sky comparison (dashed, freeze excluded) and the realistic TMY-altitude comparison at Golmud (solid, freeze included), with the 6 h reversal marked explicitly. (b) Decomposition at 6 h storage: moving from clear-sky to TMY irradiance raises both costs but *preserves* the salt's lead, whereas charging the freeze burden reverses the ranking – so freeze, not the irradiance reduction, is what makes thermal oil the cheaper option.

Table 3: LCOE under the idealized clear-sky comparison (freeze excluded) versus the realistic typical-meteorological-year comparison at Golmud (freeze included), each at the fluid's cost-optimal storage duration. The ranking reverses once the freeze burden is charged on realistic weather.

Comparison basis	Salt LCOE (CNY/MWh)	Oil LCOE (CNY/MWh)	Cheaper
Idealized clear-sky (freeze excluded)	479.6 (6 h)	523.0 (3 h)	Salt
Realistic TMY, Golmud (freeze included)	1040.5 (6 h)	867.6 (3 h)	Oil

choice.

6. Results and discussion

Across the four dimensions the fluids trade places depending on the operating scenario, and once realistic weather is admitted the ranking is clearer than the design point alone suggests.

At the design point molten salt leads – higher first- and second-law efficiency (Sections 3.2 and 3.4) and, under the idealized clear-sky comparison, a lower LCOE thanks to its cheaper direct storage (Section 5). These advantages are real but fragile, because each is evaluated before the freeze penalty is charged.

Freeze protection is where they unravel. The direct effect of altitude on heat loss is negligible (Section 3.1) and the freeze power itself is nearly altitude-independent (Section 3.3); what makes a high plateau hard for molten salt is its cold, intermittent climate. Charged on realistic typical-meteorological-year weather, the 245 MWh annual freeze burden pulls the salt's net generation below the oil's (897 versus 1073 MWh, Table 1), inverts the annual exergy ranking, and – decisively – reverses the cost ranking: the salt's LCOE rises to 1040 CNY MWh^{-1} against the oil's 868 (Table 3, Section 5.1). On the same realistic basis, then, the oil wins on energy, on annual exergy, and on cost; the salt's apparent advantages are artefacts of an idealized, freeze-free comparison.

The practical conclusion is therefore narrower, but stronger, than a generic "high altitude" rule: at the cold Golmud plateau site represented by the TMY record, thermal oil is the more economic choice, and molten salt's storage-cost advantage materialises only where winters are mild enough, or freeze mitigation is effective enough, to suppress the parasitic. The decision is governed by freeze-protection economics under cold-site operation, and the single most valuable fluid improvement is a lower-freezing-point salt that removes the parasitic – which would restore the salt's structural storage-cost advantage under real weather. The aperture-scale optical design of the collector is treated in the companion paper [15]; here the collector is held at the 5.77 m reference so that the fluid comparison is not confounded by optical scale.

Several limitations bound these results. The study demonstrates the framework at one site; the physics and the 4E/market machinery are general, but the quantitative balance would shift at a warmer or colder location, so we report a framework and a demonstration rather than a universal ranking. The cost parameters, though anchored to recent Chinese plant data, are configuration-driven and carry the usual techno-economic uncertainty; the LCOE differences we rely on are robust in sign for the tested guard margins but remain smaller than the absolute cost uncertainty of early-stage CSP estimates. Finally, the freeze model is a steady maintenance-power estimate rather than a transient simulation with field-drain, trace-heating zoning, start-up, and recirculation logic. The annual results also use a single TMY realisation. These are acceptable for ranking mechanisms, but a deployment-grade conclusion would require a site-specific transient freeze-protection model and multi-year weather sensitivity.

7. Conclusions

We have assessed heat-transfer-fluid selection for a high-altitude parabolic-trough plant using a four-dimensional (energy, exergy, economic, environmental) framework coupled to a thermal-storage market-value model, with altitude-dependent air properties propagated through heat loss, freeze protection, and exergy. The main findings are:

- The direct effect of altitude on receiver heat loss is small (∼0.2%), because reduced convective loss is offset by increased radiative loss; what altitude shifts is the loss *partitioning* (convective fraction 69% to 65% from 110 to 2801 m), which a sea-level-hardcoded model misses.

- Freeze protection is molten salt's dominant penalty – about 20 times the oil's maintenance power under the modeled guard temperatures – and is nearly altitude-independent; its consequence enters through cold, cloudy weather, reaching 245 MWh per year at Golmud under TMY and there pulling the salt's net generation below the oil's.

- Under an idealized clear-sky comparison molten salt's cheaper direct storage gives it the lower LCOE (480 versus 523 CNY MWh^{-1} at each fluid's optimum), reproducing the conventional preference. But charged on realistic TMY weather the freeze penalty reverses this: the salt's LCOE rises to 1040 CNY MWh^{-1} against the oil's 868, so under real plateau weather thermal oil is the cheaper option.

- The fluid choice at the cold Golmud plateau site is therefore governed by freeze-protection economics under realistic weather, not by air-density heat-loss correction, storage cost, or design-point conversion efficiency alone; the conventional preference for molten salt can invert, and the decisive lever is a lower-freezing-point salt.

The last point sets the priority for future work: low-melting multi-component nitrate salts, with freezing points well below that of the conventional 60–40 mixture [35] and now demonstrated at multi-megawatt scale in a trough loop [36], would directly attack the parasitic this analysis identifies as decisive and, by removing it, restore molten salt's structural storage-cost advantage under real weather. The aperture-scale optics that complement this fluid study are reported in the companion paper [15].

Nomenclature

Latin symbols

E_{net}	annual net electricity (MWh)
n	plant lifetime (yr)
p	air pressure (Pa)
$\dot{Q}$	heat-transfer rate (W)
R_a	specific gas constant of air ($\mathrm{J\,kg^{-1}\,K^{-1}}$)
r	discount rate (–)
T	temperature (K or °C)
T_0	reference (ambient) temperature
z	site elevation (m)

Greek symbols

η	overall solar-to-electric efficiency (–)
η_{ex}	exergy efficiency (–)
μ	dynamic viscosity (Pa s)
ν	kinematic viscosity ($\mathrm{m^2\,s^{-1}}$)
ρ	air density ($\mathrm{kg\,m^{-3}}$)

Abbreviations

CAPEX	capital expenditure
CHL	convective heat loss
CRF	capital recovery factor
CSP	concentrating solar power
HTF	heat-transfer fluid
LCOE	levelized cost of energy
O&M	operation and maintenance
RHL	radiative heat loss
TMY	typical meteorological year

Declaration of generative AI and AI-assisted technologies in the manuscript preparation process

During the preparation of this work the authors used ChatGPT (OpenAI) and Claude (Anthropic) to assist with programming and computation, language editing of the manuscript, and organising and producing figures. No AI tool was used to generate the underlying simulation data or model, or to draw the scientific conclusions, which are the authors' own. After using these tools, the authors reviewed and edited the content as needed and take full responsibility for the content of the published article.

CRediT authorship contribution statement

Zhaohui Han: Conceptualization, Methodology, Formal analysis, Visualization, Writing – original draft. **Zengli Dai:** Supervision, Resources, Funding acquisition, Writing – review & editing. **Yuan Wei:** Methodology, Supervision, Project administration. **Yu Xie:** Investigation, Writing – review & editing, Software. **Dongxiang Wang:** Validation, Data curation, Writing – review & editing. All authors have read and agreed to the published version of the manuscript.

Declaration of competing interest

The authors are employed by SEPCOIII Electric Power Construction Co., Ltd. This research was funded by POWERCHINA GROUP (grant number DJ-ZDXM-2025-19), the parent company of SEPCOIII Electric Power Construction Co., Ltd. The authors declare no other financial interests or personal relationships that could have appeared to influence the work reported in this paper.

Funding

This research was funded by POWERCHINA GROUP, grant number DJ-ZDXM-2025-19.

Data availability

The simulation code (`msptc`) is openly available at `https://github.com/han348661657/msptc` (MIT License) and archived at Zenodo (DOI: `https://doi.org/10.5281/zenodo.20896806`). The archived package contains the model source code, default configuration, and the analysis and plotting scripts that regenerate the figures and derived source tables reported here. The proprietary hourly TMY weather file used for the Golmud simulations is not redistributed because the SolarGIS data license does not permit public transfer of the original data. Licensed users can reproduce the TMY cases by placing an equivalent TMY3 file at `data/CHN_QH_GEERMU_TMY3.csv` or by passing `-tmy-file`. The TMY-derived analyses cite the source as Data services © Solargis, with the delivery year retained in the archived package.

Acknowledgements

The authors acknowledge the open technical documentation and reference implementations from NREL, IRENA, IEA, and the broader concentrating-solar-power research community that made the model comparison reproducible.

References

[1] H. Price, E. Lüpfert, D. Kearney, E. Zarza, G. Cohen, R. Gee, R. Mahoney, Advances in parabolic trough solar power technology, Journal of Solar Energy Engineering 124 (2) (2002) 109–125. doi:10.1115/1.1467922.

[2] A. Fernández-García, E. Zarza, L. Valenzuela, M. Pérez, Parabolic-trough solar collectors and their applications, Renewable and Sustainable Energy Reviews 14 (7) (2010) 1695–1721. doi:10.1016/j.rser.2010.03.012.

[3] S. A. Kalogirou, Solar thermal collectors and applications, Progress in Energy and Combustion Science 30 (3) (2004) 231–295. doi:10.1016/j.pecs.2004.02.001.

[4] K. Vignarooban, X. Xu, A. Arvay, K. Hsu, A. M. Kannan, Heat transfer fluids for concentrating solar power systems – a review, Applied Energy 146 (2015) 383–396. doi:10.1016/j.apenergy.2015.01.125.

[5] D. Kearney, U. Herrmann, P. Nava, B. Kelly, R. Mahoney, J. Pacheco, R. Cable, N. Potrovitza, B. Blake, H. Price, Assessment of a molten salt heat transfer fluid in a parabolic trough solar field, Journal of Solar Energy Engineering 125 (2) (2003) 170–176. doi:10.1115/1.1565087.

[6] U. Herrmann, D. W. Kearney, Survey of thermal energy storage for parabolic trough power plants, Journal of Solar Energy Engineering 124 (2) (2002) 145–152. doi:10.1115/1.1467601.

[7] B. Lynch, H. Metghalchi, Y. Levendis, Concentrating solar thermal power in china: 2025 review and outlook, ASME Open Journal of Engineering 4 (2025) 040807. doi:10.1115/1.4070013.

[8] National Solar Thermal Power Industry Technology Innovation Strategic Alliance and China Renewable Energy Society, Blue book of china's concentrating solar power industry, Advanced Technology of Electrical Engineering and Energy 45 (2) (2025) 1–45. doi:10.12067/ATEEE2601019.

[9] M. McPherson, M. Mehos, P. Denholm, Leveraging concentrating solar power plant dispatchability: A review of the impacts of global market structures and policy, Energy Policy 139 (2020) 111335. doi:10.1016/j.enpol.2020.111335.

[10] J. Jorgenson, P. Denholm, M. Mehos, C. Turchi, Estimating the performance and economic value of multiple concentrating solar power technologies in a production cost model, Tech. Rep. NREL/TP-6A20-58645, National Renewable Energy Laboratory (2013). doi:10.2172/1078779.

[11] P. Alamdari, M. Khatamifar, W. Lin, Heat loss analysis review: Parabolic trough and linear fresnel collectors, Renewable and Sustainable Energy Reviews 199 (2024) 114497. doi:10.1016/j.rser.2024.114497.

[12] D. Wang, B. Fan, Y. Chen, Y. Han, Y. Liu, Y. Wang, H. Liu, X. Jiao, Comparative analysis of heat loss performance of flat plate solar collectors at different altitudes, Solar Energy 244 (2022) 490–506. doi:10.1016/j.solener.2022.08.060.

[13] Z. Said, M. Ghodbane, B. Boumeddane, A. K. Tiwari, L. S. Sundar, C. Li, N. Aslfattahi, E. Bellos, Energy, exergy, economic and environmental (4e) analysis of a parabolic trough solar collector using MXene based silicone oil nanofluids, Solar Energy Materials and Solar Cells 239 (2022) 111633. doi:10.1016/j.solmat.2022.111633.

[14] S. K. Singh, A. K. Tiwari, Z. Said, MXene nanofluid enhanced parabolic trough collectors: An integrated energy, exergy, environmental, and economic study, Solar Energy 276 (2024) 112658. doi:10.1016/j.solener.2024.112658.

[15] Z. Han, Error-cone intercept modeling and altitude–wind-load synergy in large-aperture (8.6 m) parabolic-trough collectors, Companion paper, under review, companion manuscript (2026).

[16] C. A. Gueymard, REST2: High-performance solar radiation model for cloudless-sky irradiance, illuminance, and photosynthetically active radiation – validation with a benchmark dataset, Solar Energy 82 (3) (2008) 272–285. doi:10.1016/j.solener.2007.04.008.

[17] S. Wilcox, W. Marion, Users manual for TMY3 data sets, Tech. Rep. NREL/TP-581-43156, National Renewable Energy Laboratory (2008). doi:10.2172/928611.

[18] NOAA and NASA and USAF, U.s. standard atmosphere, 1976, Tech. Rep. NOAA-S/T 76-1562, U.S. Government Printing Office (1976).

[19] W. Sutherland, The viscosity of gases and molecular force, Philosophical Magazine 36 (223) (1893) 507–531. doi:10.1080/14786449308620508.

[20] W. C. Swinbank, Long-wave radiation from clear skies, Quarterly Journal of the Royal Meteorological Society 89 (381) (1963) 339–348. doi:10.1002/qj.49708938105.

[21] P. Berdahl, M. Martin, Emissivity of clear skies, Solar Energy 32 (5) (1984) 663–664. doi:10.1016/0038-092X(84)90316-3.

[22] R. Forristall, Heat transfer analysis and modeling for a parabolic trough solar receiver implemented in engineering equation solver, Tech. Rep. NREL/TP-550-34169, National Renewable Energy Laboratory (2003). doi:10.2172/15004820.

[23] F. Burkholder, C. Kutscher, Heat loss testing of schott's 2008 PTR70 parabolic trough receiver, Tech. Rep. NREL/TP-550-45633, National Renewable Energy Laboratory (2009). doi:10.2172/1369635.

[24] F. P. Incropera, D. P. DeWitt, T. L. Bergman, A. S. Lavine, Fundamentals of Heat and Mass Transfer, 7th Edition, John Wiley & Sons, 2011.

[25] S. W. Churchill, M. Bernstein, A correlating equation for forced convection from gases and liquids to a circular cylinder in crossflow, Journal of Heat Transfer 99 (2) (1977) 300–306. doi:10.1115/1.3450685.

[26] A. B. Zavoico, Solar power tower design basis document, revision 0, Tech. Rep. SAND2001-2100, Sandia National Laboratories (2001). doi:10.2172/786629.

[27] R. W. Bradshaw, N. P. Siegel, Molten nitrate salt development for thermal energy storage in parabolic trough solar power systems, in: Proc. ASME 2nd Int. Conf. Energy Sustainability (ES2008-54174), 2008. doi:10.1115/ES2008-54174.

[28] V. Russo, G. Napoli, F. Rovense, P. Di Ascenzi, G. Giorgi, L. Mongibello, C. Cancro, G. Ciniglio, W. Gaggioli, Investigations on solidification and melting processes of the solar salt mixture in evacuated and non-evacuated receiver tubes, Energies 18 (17) (2025) 4492. doi:10.3390/en18174492.

[29] N. Khandelwal, P. S. Yadav, Z. Said, M. Sharma, A. K. Shukla, O. Singh, D. Khandelwal, H. Caliskan, A comprehensive analysis of energy, exergy, economic and environment on integrated solar-combined cycle with various htfs and thermal storage, Applied Energy 376 (2024) 124203. doi:10.1016/j.apenergy.2024.124203.

[30] R. Petela, Exergy of undiluted thermal radiation, Solar Energy 74 (6) (2003) 469–488. doi:10.1016/S0038-092X(03)00226-3.

[31] J. Szargut, D. R. Morris, F. R. Steward, Exergy Analysis of Thermal, Chemical, and Metallurgical Processes, Hemisphere Publishing, 1988.

[32] C. S. Turchi, G. A. Heath, Parabolic trough reference plant for cost modeling with the solar advisor model (sam), Tech. Rep. NREL/TP-5500-57625, National Renewable Energy Laboratory (2013). doi:10.2172/1067902.

[33] International Renewable Energy Agency, Renewable power generation costs in 2020, Tech. rep., IRENA, iSBN 978-92-9260-282-6 (2021).

[34] International Energy Agency, CO2 emissions from fuel combustion: Overview, Tech. rep., IEA, https://www.iea.org/data-and-statistics (2022).

[35] H. Wang, J. Wei, L. Luo, J. Wang, J. Xu, J. Yin, S. Ma, G. Zhao, Thermophysical properties and phase diagram analysis of binary, ternary and quaternary nitrates for thermal energy storage applications, Solar Energy 286 (2025) 113151. doi:10.1016/j.solener.2024.113151.

[36] N. Dicke, M. Meyer-Grünefeldt, M. Wittmann, J. Stengler, P. Horta, P. Martins, et al., Demonstration of 3.5 MWth parabolic trough with ternary molten salt at the évora molten salt platform, in: SolarPACES Conference Proceedings, Vol. 1, 2024. doi:10.52825/solarpaces.v1i.640.